Theor Appl Climatol
DOI 10.1007/s00704-015-1510-2

ORIGINAL PAPER

Internal evaporation and condensation characteristics in the shallow soil layer of an oasis

Yinhuan Ao[1] · **Bo Han**[1] · **Shihua Lu**[1] · **Zhaoguo Li**[1,2]

Received: 9 November 2014 / Accepted: 12 May 2015

Abstract The surface energy balance was analyzed using observations from the Jinta oasis experiment in the summer of 2005. A negative imbalance energy flux was found during daytime that could not be attributed to the soil heat storage process. Rather, the imbalance was related to the evaporation within the soil. The soil heat storage rate and the soil moisture variability always showed similar variations at a depth of 0.05 m between 0800 and 1000 (local standard time), while the observed imbalanced energy flux was very small, which implied that water vapor condensation occurred within the soil. Therefore, the distillation in shallow soil can be derived using reliable surface energy flux observations. In order to show that the importance of internal evaporation and condensation in the shallow soil layer, the soil temperatures at the depths of 0.05, 0.10, and 0.20 m were reproduced using a one-dimensional thermal diffusion equation, with the observed soil temperature at the surface and at 0.40 m as the boundary conditions. It was found that the simulated soil temperature improves substantially in the shallow layer when the water distillation is added as a sink/source term, even after the soil effective thermal conductivity has been optimized. This result demonstrates that the process of water distillation may be a dominant cause of both the temperature and moisture variability in the shallow soil layer.

✉ Bo Han
hanbo@lzb.ac.cn

[1] Key Laboratory of Land Surface Process and Climate Change in Cold and Arid Regions, Cold and Arid Regions Environmental and Engineering Research Institute, Chinese Academy of Sciences, 730000 Lanzhou, China

[2] University of Chinese Academy of Sciences, 100049 Beijing, China

1 Introduction

Surface energy fluxes determine the development of the atmospheric boundary layer (Moeng and Sullivan 1994) and thus affect the local and global climate (Garratt 1994). Much research in this field has focused on land–air interactions (Beltrán-Przekurat et al. 2012; Culf et al. 2004; Heusinkveld et al. 2004; Oke et al. 1999; Wilson et al. 2002; Wu et al. 2007), and, among these works, the surface energy balance over different kinds of underlying surface has always been the primary concern.

On Earth, the energy fluxes should be in balance according to the relationship

$$R_n - G_0 = H_s + lE_s, \quad (1)$$

where R_n is the net radiation flux at the land surface, G_0 is the surface soil heat flux, and H_s and lE_s are the surface sensible and latent heat fluxes, respectively. In this study, l was set to be 2.5×10^6 J kg^{-1}, and thus, the evaporation (or evapotranspiration—considered the same as evaporation in this study) rate was proportional to the latent heat flux. Equation 1 should always be correct because all energy fluxes within it are absorbed (R_n) or released (G_0, H_s, and lE_s) at the land surface, and the capacity of the land surface should always be zero. However, in situ observations, H_s and lE_s, are usually recorded at specific heights using an eddy covariance system, and the soil heat flux plate needs to be placed at a specific depth also. As a result, what we actually observe is the energy flux entered into a system consisting of a column of air and soil and the encompassed canopy. Therefore, the observed energy fluxes are usually imbalanced. The imbalanced energy flux (R) is given by

$$R = R_n - G_{ref} - H_s - lE, \quad (2)$$

where G_{ref} is the soil heat flux at a certain reference depth (z_{ref}) and lE is the observed latent energy flux. Being different from

Published online: 24 May 2015

lE_s, the latent heat flux due to internal evaporation can also contribute to lE and will be discussed in this paper. Because the observed system possesses a nonzero heat capacity, the energy change within it can induce R (Heusinkveld et al. 2004; Jacobs et al. 2008; Yang and Wang 2008).

If thermal conduction is the main mechanism for energy transport within the soil in the vertical direction, and there is no significant horizontal heat transfer process, then the following equation should hold:

$$S \equiv \int_{z=0}^{z=z_{\mathrm{ref}}} \rho_s c_s \frac{\partial T}{\partial t} dz = G_0 - G_{\mathrm{ref}}, \tag{3}$$

where S is the soil heat storage rate. If $E_s \approx E$, from Eq. 2, R should be close to S. This simple case indicates that analysis of the surface energy balance is connected to shallow-soil thermal variations. In fact, some processes—being difficult to be monitor directly—can be evaluated from analysis of the surface energy of the land; for example, dew on the land surface or canopy (Agam and Berliner 2006; Ninari and Berliner 2002). However, when thermal conduction no longer presents the main heat transfer within soil, R may no longer be determined by S.

Being different from the surface latent heat flux, the water vapor flux generated from the evaporation within soil pores (internal evaporation hereafter) cannot currently be measured directly. Some studies have reported that internal evaporation contributes significantly to the observed surface evaporation in loose and unsaturated soil (vadose zone) (Massmann and Farrier 1992; Milly 1984; Ong et al. 1992; Saito et al. 2006; Zeng et al. 2009). The process of internal evaporation demands a much more complicated experimental representation compared to that of surface evaporation flux (Monteith 1965; Penman 1948), although its mechanism can be well described by conceptual models (Kondo et al. 1990; Philip 1957; Philip and De Vries 1957).

Similar to internal evaporation, the condensation of water vapor (dew), whether on the canopy or within the soil pores—a process identified in many studies as an important water supplement in arid regions (Agam and Berliner 2006; Andrade 2003; Garratt and Segal 1988; Jacobs et al. 1990, 1999, 2006, 2008)—is also difficult to monitor. Some results show that the turbulence-induced latent energy flux should be negative when the amount of dew exceeds the rate of evaporation (Agam and Berliner 2006; Jacobs et al. 2008); however, the inability of an eddy covariance system to measure the turbulence at night has also been noted (Jacobs et al. 2008). Thus, the amount of dew is usually measured by detecting the change in soil weight and infiltrated water using a lysimeter (Fritschen and Doraiswamy 1973; Richards 2004; Sharma 1976; Waggoner et al. 1969; Xiao et al. 2009). Obviously, this method is efficient for evaluating the total water exchange between a box of soil and its surroundings, but it is unable to accurately evaluate the water exchange between soil layers (like water distillation).

The process of water distillation within soil is suggested to be important when the soil temperature gradient is steep (Bouddour et al. 1998; De Vries 1958; De Vries and Philip 1986; Deru and Kirkpatrick 2002; Philip and De Vries 1957) and is closely connected with soil hydrothermal variations (Johnson et al. 2003; Ren et al. 2008; Shao and Irannejad 1999; Yang et al. 2005). A mass–heat coupled model should be able to provide a full description of the movement of liquid and gaseous water, as well as their phase transition, and indeed, some of the reported results from such models seem to be comparative with laboratory observations (Gao 2005; Gao et al. 2003; Henry 2007, 2008; Li and Sun 2008; Olivella et al. 2000; Poutou et al. 2004; Saito et al. 2006; Sakai et al. 2009; Simunek et al. 2008). Within these studies, an effective thermal conductivity is usually used to represent the heat transfer generated from both pure thermal conduction and other processes, such as the water distillation within soil (De Vries and Philip 1986; Devries 1987; Heitman and Horton 2011; Johansen 1977; Nassar et al. 1992; Sundberg 1988; Tarnawski et al. 2000; Wang et al. 2007).

If the rate of water distillation is strong, then a more detailed description of water vapor movement mainly results from the dependence of the water vapor pressure (or concentration) on temperature and water potential. In this case, the distillation process can be expressed as the divergence/convergence of the derived water vapor flux. However, it should be noted that, usually, only the calculated/simulated soil temperature, moisture, heat flux, or chemical tracer content, rather than the rate of water distillation itself, can be compared with observations (Grifoll et al. 2005; Heitman and Horton 2011; Sakai et al. 2009; Scanlon 1992, 1994; Scanlon and Milly 1994). Among these studies, only a few considered the potential effect of water distillation on the heat or mass transfer within soil (Bittelli et al. 2008; Bouddour et al. 1998).

The prerequisite for using a mass–heat coupled model is that certain critical relations, such as the retention curve and the soil thermal and hydrological conductivity functions, are already known. This is usually a tough task for a field experiment focusing on land–air interaction, like the Jinta experiment mentioned in this study. Moreover, to assume the soil column as bundles of capillary tubes, as in most heat–mass coupled soil models, has also been criticized, for being unrealistic (Hunt et al. 2013; Tuller et al. 1999). Because of the weaknesses of soil models and observations, there has been little research conducted on land surface processes in which proper consideration has been given to the distillation within soil, especially in the shallow-soil layer.

Therefore, to discuss the importance of distillation within shallow soil, we first needed to clarify how the internal evaporation and condensation taking place in shallow soil impact

the observed surface energy flux. Having done this, an approach to describe the distillation in shallow soil was developed. To investigate the rationality of the approach, the soil temperature was reproduced using a one-dimensional thermal diffusion equation. We report our findings in the present paper as follows: In Section 2, a brief introduction to the observational experiment is given. In Section 3, the balance between observed energy fluxes on the land surface is investigated. The effect of internal evaporation and condensation on the surface energy balance is discussed in Section 4. The results from a simple one-dimensional thermal diffusion equation are given in Section 5. Finally, some further discussion and the main conclusions are presented in Sections 6 and 7, respectively.

2 Jinta experiment

The Jinta oasis is located in the western Badain Jaran desert, along the middle reaches of the Heihe river (98° 39′–99° 08′ E, 39° 56′–40° 17′ N; approximately equal to 1500 m above sea level), with an area of approximately 2152 km^2 (Fig. 1). It is a typical semiarid region in northwest China, being surrounded by deserts and the Gobi (Qi et al. 2007). The Heihe river basin is a popular site for researching land–air interaction (Bastiaanssen et al. 1998; Tsukamoto et al. 1995; Wang and Mitsuta 1992). More information on the location and landscape of the Jinta oasis can be found in Chu et al. (2005). The atmospheric optical depth is so short in this region that the maximum irradiance at the land surface is larger than 1300 W m^{-2} in summer. This causes high potential evaporation at around 2538 mm year^{-1}. By contrast, the precipitation rate is rather low, being approximately 60 mm year^{-1}. Replenishment of the soil water relies mainly on the Heihe river and underground water.

The water exchange between the soil and atmosphere in the Jinta oasis is peculiarly intense because of the high level of potential evaporation and the plentiful soil water supply. Moreover, the soil pore space is large because of the regular human (agricultural) activity that takes place in the area. Hence, water vapor can move freely in the vertical direction as in the vadose zone (Massmann and Farrier 1992; Milly 1984; Ong et al. 1992; Saito et al. 2006; Zeng et al. 2009). All these conditions are conducive to the occurrence of internal evaporation within the soil.

The observation site (39° 59.488′ N, 98° 56.177′ E) is located in an irrigated field of spring wheat. The observations were taken from June 17 to July 8, 2005. Since the field is flat and well plowed, the soil features near the observation site can be considered as horizontally homogeneous. There was no precipitation during the observation period, but the field was irrigated on the morning of June 22. Therefore, the data from 0000 (LST, the same hereafter) June 26 to 0000 July 7 were

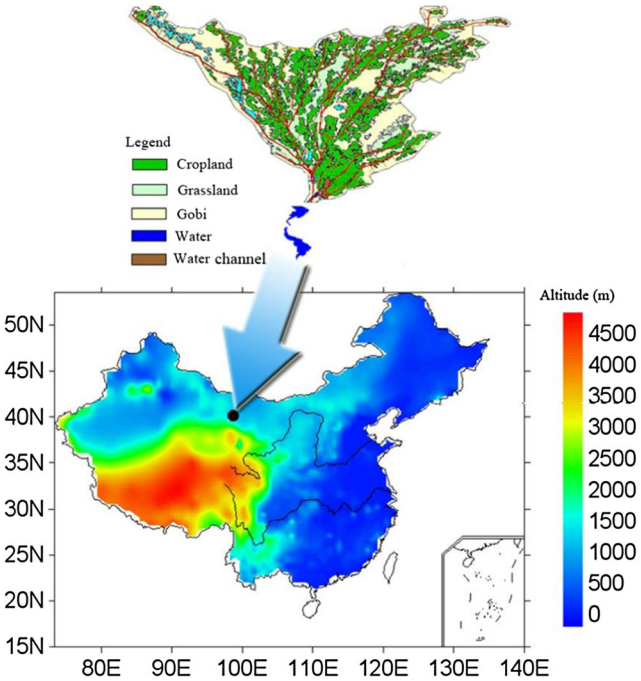

Fig. 1 Geographical and land-use sketch map of the Jinta oasis (Ao, et al. 2014)

chosen for this study. The observational instruments are listed in Table 1. The eddy covariance system contains a three-dimensional sonic anemometer and an H_2O analyzer, with a sampling frequency of 10 Hz. The turbulent energy fluxes were calculated and stored every 10 min. The observational data were subjected to necessary quality control, but no subjective selection was applied to the data so as to guarantee the representativeness of the conclusions.

3 Surface energy flux balance analysis

The observed surface energy flux is given in Fig. 2. It is easy to see that most of the surface net radiation (R_n) is converted into latent energy (lE) during daytime; the sensible heat flux (H_s) is smaller than the soil heat flux (G_{ref}). A greater surface soil heat flux (G_0) can be expected during daytime (Eq. 3), which indicates that the energy transport within the soil is particularly intense in the oasis farmland. The intense soil heat flux provides the energy for internal evaporation, which may sequentially induce the internal condensation. Because there are no reliable methods to directly monitor the phase transition processes of water within soil, we first turn to analyze the surface energy balance.

The imbalance energy flux (R) is easy to calculate from Eq. 2. The imbalance has various potential causes, e.g., secondary circulation due to a nonuniform underlying surface (Han et al. 2010) and atmospheric low-frequency fluctuations (Sakai et al. 2001). If the surface energy fluxes are properly

Table 1 Instrument and measurement height for the Jinta experiment

Observation instrument	Model	Manufacturer	Probe height/depth (m)
3-D sonic anemometer	CSAT3	Campbell	3.20
H_2O analyzer	KH20	Campbell	3.20
Net radiometer	CNR1	Kipp & Zonen	1.50
Soil temperature sensor	107 L	Campbell	−0.05
			−0.10
			−0.20
			−0.40
Soil water content sensor	CS616	Campbell	−0.05
			−0.10
			−0.20
Soil heat flux plate	HFP01	Hukseflux	−0.05

observed, and there is no other energy transport process between the observed system and its environment, then S should, from Eqs. 2 to 3, be the main contributor to R. Indeed, such a result has been confirmed in many previous studies (Culf et al. 2004; Foken 2008; Foken et al. 2010), especially in bare soil over semiarid regions (Heusinkveld et al. 2004; Oncley et al. 2007). Thus, we also expected similar results in the Jinta experiment.

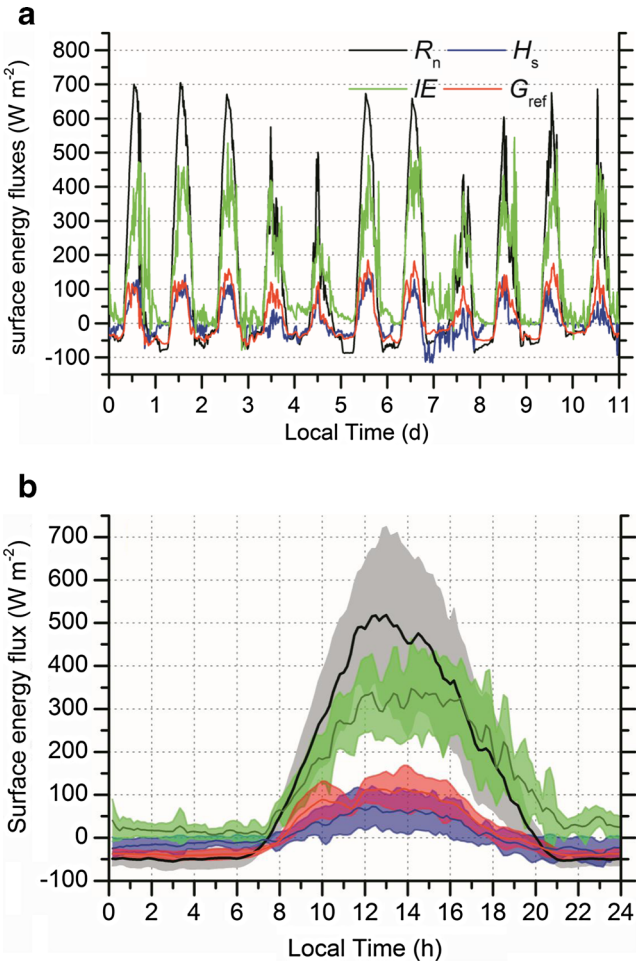

Fig. 2 Observed daily variations of the surface energy flux from 0000 June 27 to 0000 July 8 (**a**) and their daily averaged diurnal variations (**b**). The lines in **b** are the same as those indicated by the legend in **a** but for the diurnal averaged value. A 7-point smoothing has been applied in both **a** and **b**. The colors represent the standard deviation for each moment in a day

From Eq. 3, using the observed soil temperature, S can be approximately calculated by

$$S \approx \frac{1}{2}\left(\frac{\partial}{\partial t}T_{sfc} + \frac{\partial}{\partial t}T_{05}\right)\rho_s c_s z_{ref}, \tag{4}$$

where T_{05} is the soil temperature at a depth of 0.05 m, and ρ_s and c_s are the density and heat capacity of the soil, respectively. The quantity T_{sfc} is the land surface temperature, which is derived from the Stefan–Boltzmann relationship to be

$$T_{sfc} = \left(\frac{R_{lu} - (1-\varepsilon_g)R_{ld}}{\varepsilon_g \sigma}\right)^{1/4}, \tag{5}$$

where ε_g=0.98 is the surface emissivity; R_{lu} and R_{ld} are the upward and downward long-wave radiative fluxes at the land surface, respectively, and $\sigma = 5.67\times10^{-8}$ (W m^{-2} K^{-4}) is the Stefan–Boltzmann constant. The volumetric capacity of moistened soil, $\rho_s c_s$, is given by the following relationships:

$$\rho_s c_s = \rho_{dry} c_{dry} \theta_{sat} + \rho_w c_w \theta. \tag{6}$$

Here, θ_{sat} is the soil porosity, equal to 0.6 for all soil layers, which is derived from the observed volumetric soil water content, θ (m^3 m^{-3}). The quantities $\rho_{dry}c_{dry}$ and $\rho_w c_w$ are the volumetric capacities of dry soil and liquid water, set to be 2.2×10^6 and 4.2×10^6 J K^{-1} m^{-3}, respectively. Note that although the soil heat capacity is given empirically, it did not affect the simulations described in Section 5.

The variations of R and S are given together in Fig. 3, as computed by Eqs. 3–6. Obviously, R and S possess quite different phases, especially from their daily averaged diurnal variation (Fig. 3b): before 1200, when S reaches its maximum value at 0900, R is generally small, and even negative;

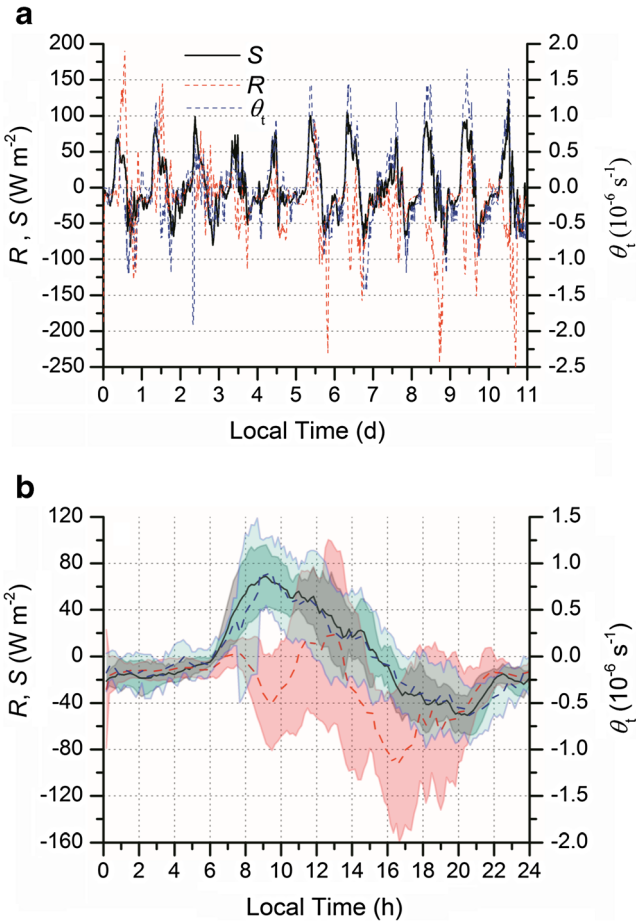

Fig. 3 As in Fig. 2 but for the residual energy flux (R, *red dashed line*), soil heat storage (S, *black solid line*) and moisture variability at a depth of 0.05 m (θ_t, *blue dashed line*)

between 1200 and 1800, although they are both decreasing, R is still much smaller than S. Such results indicate that the energy transport in soils may not just rely on thermal conduction, according to Eq. 3.

Coincidently, the soil moisture variability (θ_t) at a depth of 0.05 m shows almost identical variation as S (Fig. 3). From Fig. 4, the correspondence between S and θ_t is more robust than that between S and R during the entire observation period. In other words, the process of heating (cooling) and moistening (drying) in upper shallow soil seems to take place simultaneously. Because the heating–moistening process corresponds naturally to condensation, and the cooling–drying process to evaporation, the rate of water distillation seems to be reflected in the surface energy flux analysis.

4 Internal evaporation/condensation in soil

To help understand the energy transfer in loose soil during daytime, a schematic diagram is given as Fig. 5. Here, the heat storage in air and plants was ignored, so the capacity of the

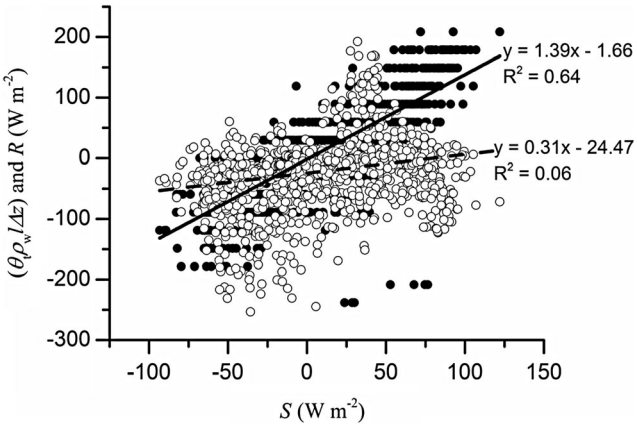

Fig. 4 The soil heat storage rate (S, from Eq. 3) against the energy change corresponding to soil moisture variability ($\theta_t\rho_w l$ from Eq. 15, *filled circles*) and that against the residual energy flux (R in Eq. 2, *open circles*), every 10 min, from the Jinta experiment. Their linear fitted functions are also given as a solid ($\theta_t\rho_w l$ vs. S) and dashed line (R vs. S), respectively

observed system was approximately equal to that of the soil column between the land surface (Z_0) and Z_{ref} (0.05 m).

4.1 Internal evaporation

When internal evaporation is considered, the observed latent heat flux (lE) can be divided into two portions:

$$lE = lE_s + lE_i'. \tag{7}$$

Here, E_i' is the vertical vapor flux generated by internal evaporation in soil pores and delivered upward by molecular diffusion (Kondo et al. 1990). At the level of Z_{ref}, E_i is the vertical vapor flux. The direct energy supplement for lE_i (or lE_i') is not from radiation at the land surface but by the loss of internal energy within the soil, i.e., the evaporation-induced cooling process, although the soil heat flux may compensate for the energy loss within the soil.

In the soil layer between the surface and Z_{ref}, when the internal evaporation-induced vapor flux, E_{ic}, has been considered, its internal energy control equation can be written as

$$S \equiv c_s\rho_s \int_{Z=0}^{Z=Z_{ref}} \frac{dT}{dt} dZ = G_0 - G_{ref} - lE_{ic}. \tag{8}$$

Therefore, Eq. 3 is no longer true in this situation. By putting Eqs. 7 and 8 into Eq. 2, R can be calculated by

$$\begin{aligned} R \equiv R_n - G_{ref} - H_s - l(E_s + E_i') &= (R_n - G_0 - H_s - lE_s) \\ &+ S + lE_{ic} - lE_i' = S + lE_{ic} - lE_i'. \end{aligned} \tag{9}$$

Thus, besides soil heat storage, the latent heat flux from internal evaporation in the soil also contributes to the observed imbalanced energy flux.

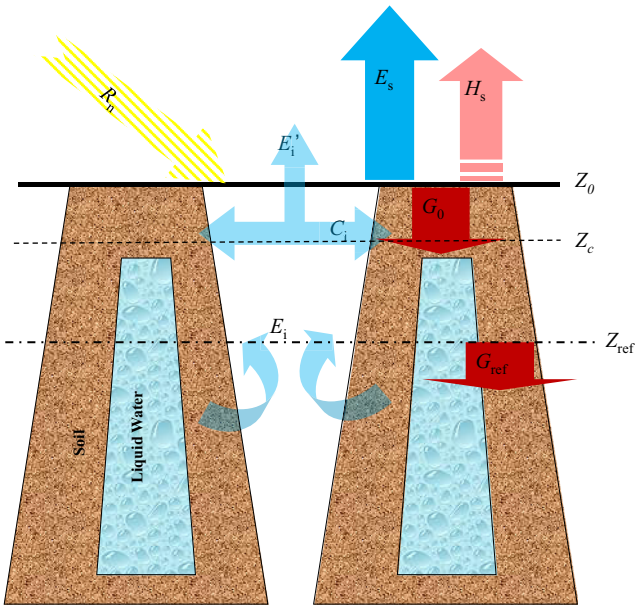

Fig. 5 Vertical cross-section of the soil–atmosphere energy transfer during the daytime at the Jinta experiment site. *Arrows* represent the energy fluxes. On the land surface, there is surface net radiation flux (R_n), surface evaporation flux (E_s), surface sensible heat flux (H_s), surface soil heat flux (G_0), and water vapor flux from internal evaporation (E_i'). The energy fluxes within the soil are internal evaporation flux (E_i), internal condensation flux (C_i), and soil heat flux (G_{ref}). The latent heat coefficient (l) has been ignored. There are three levels noted: Z_0, land surface; Z_c, the depth where condensation always takes place; and Z_{ref}, where the soil heat flux plate was buried (0.05 m) during the experiment

If there is no condensation in the soil and the vapor density in the soil is constant, then the following is valid:

$$E_{ic} = E_i' - E_i. \tag{10}$$

With the assumption that the soil temperature change is rather small ($S \approx 0$), from Eqs. 9 to 10, R should be close to $-lE_i$. Therefore, the more significant the internal evaporation is that takes place below Z_{ref}, the more negative the imbalanced energy flux will be. This phenomenon can be seen in the observation at 1630 in Fig. 3b. During the observation period, the daily averaged R was −24.22 W m^{-2}, which may be comparable to the daily averaged latent heat flux from the internal evaporation there. Moreover, during the observation period (11 days), little change was observed in the daily mean soil moisture at 0.05 m (Fig. 7), but the soil moisture at a depth of 0.20 m decreased from approximately 0.50 to 0.35 m^3 m^{-3}. The capillary process can also contribute to the drying process in deeper soil. Its effect is discussed later in Section 6.

If the internal evaporation mainly takes place above Z_{ref} ($E_i \approx 0$), then $E_{ic} \approx E_i'$. From Eq. 3 to 9, R still equals S. However, the internal evaporation still contributes to the observed latent energy flux in this situation. Because an underestimation of G_0 will be given if Eq. 3, rather than Eq. 8, was used, this counteracts the overestimation of lE_s (because here lE is used) and makes R identical to S. This can explain why the internal evaporation has seldom been noted in many previous studies.

Generally speaking, when internal evaporation occurs, there is a source of latent energy flux (lE_i') in deeper soil layers. Because this part of the vapor flux cannot be distinguished from those generated at the land surface (lE_s), the surface energy balance equation cannot be properly verified from observations.

4.2 Internal condensation

When internal condensation (C_i) occurs in shallow soil, similar to Eq. 8, the conservation of energy in soil must hold

$$S \equiv c_s \rho_s \int_{Z=0}^{Z=Z_{ref}} \frac{dT}{dt} dZ = G_0 - G_{ref} + lE_i - lE_i' = G_0 - G_{ref} + lC_i. \tag{11}$$

Here, we assume that the density of water vapor in the soil pore space is constant so that the intensity of condensation C_i should be equal to the difference between E_i and E_i'. From Eq. 11, the imbalanced energy flux should be

$$R \equiv R_n - G_{ref} - H_s - l(E_s + E_i') = S - lC_i - lE_i'. \tag{12}$$

Obviously, R will be reduced by condensation even if S is great. For an idealized case, (1) E_i' is zero, which means that the water vapor from internal evaporation in deep soil has all been condensed near a certain level ($Z = Z_c$, as in Fig. 5) and (2) the variation of soil temperature is mainly determined by condensation, $S \approx lC_i$, meaning R should then be close to zero, according to Eq. 12. This perfectly reflects the small R but great S for the period between 0800 and 1200 in Fig. 3b. For this situation, the internal condensation, internal evaporation, and thermal conduction form an energy circle between shallow and deep soil. When condensation occurs above the soil heat flux plate ($Z_c < Z_{ref}$, as in Fig. 5), this energy circle transports a considerable amount of latent energy into the observed system from deeper soil layers.

When internal evaporation and condensation happen simultaneously, the soil heat storage rate is

$$S \equiv c_s \rho_s \int_{Z=0}^{Z=Z_{ref}} \frac{dT}{dt} dZ = G_0 - G_{ref} - lE_{ic} + lC_i. \tag{13}$$

If the variability of the total soil moisture in the layer between $Z = 0$ and $Z = Z_{ref}$ is mainly modulated by internal evaporation and condensation, it follows

$$\int_{Z=0}^{Z=Z_{ref}} \theta_t dZ \equiv \int_{Z=0}^{Z=Z_{ref}} \frac{d\theta}{dt} dZ = \frac{p(C_i - E_{ic})}{\rho_w}, \tag{14}$$

where p is a proportionality coefficient. Assuming that the difference between G_0 and G_{ref} is very small, substituting Eq. 14 into Eq. 13 gives

$$S = l\rho_w p \int_{Z=0}^{Z=Z_{ref}} \theta_t dZ \approx l\rho_w p\theta_t\Big|_{Z=Z_{ref}} \Delta Z, \quad (15)$$

where ΔZ=0.05 m. Equation 15 partly explains the identical variation of S and θ_t in Fig. 3. From the slope of the fitted line in Fig. 4, and with the assumption that the soil moisture variability is identical above a depth of 0.05 m, p should be about 71 %. Therefore, we suggest that the observed thermal variation of shallow soil is mainly determined by the water distillation within it, although other process like capillary action or film absorption may also be important. What we believe to be the most important finding is that it is improper to derive G_0 using Eq. 3 when the water distillation is intense in shallow soil.

From the above discussion, the intensity of internal evaporation and condensation can be evaluated from the shallow soil moisture variability. Whether such an approach is still useful in a soil temperature equation is discussed in the next section.

5 Numerical simulations

Although there are many powerful hydrological models (e.g., HYDRUS-1D (Saito et al. 2006)) that can give a full description of the water and energy transfer in soil, a simple model based on a one-dimensional soil thermal diffusion equation (TDE hereafter) was chosen in this study. This is because, even for a perfect model, it can only reproduce the soil hydrothermal variations properly if the soil features, such as the retention curve and the thermal and hydrological conductivity, etc., all of which have not been consistently measured in the Jinta experiment, are known and properly represented. It should also be noted that a bias of about 10 K for soil temperature and 0.1 m^3 m^{-3} for soil moisture is common in simulations using a mass–heat coupled soil model (Bittelli et al. 2008; Grifoll et al. 2005; Scanlon 1992). This would bring great uncertainty to the discussion on the significance and intensity of water distillation.

The TDE concerns the heat fluxes forced by the temperature gradient in soil. Besides pure thermal conduction, the linear part of the liquid and vapor water fluxes induced by the thermal gradient will also be involved if an effective thermal conductivity has been selected (De Vries and Philip 1986; Devries 1987; Heitman and Horton 2011; Johansen 1977; Nassar et al. 1992; Sundberg 1988; Tarnawski et al. 2000; Wang et al. 2007). Moreover, since the observational analysis revealed a simple way to present the rate of water distillation (Eq. 15), it would be interesting to see whether such a relation can improve the simulation of soil temperature, even after a proper effective thermal conductivity has been selected.

5.1 Thermal diffusion equation

The formation of the TDE is given by

$$\frac{\partial \rho_s c_s T}{\partial t} = \frac{\partial}{\partial z}\left(\lambda_s \frac{\partial T}{\partial z}\right), \quad (16)$$

$$G \equiv \lambda_s \frac{\partial T}{\partial z}. \quad (17)$$

where λ_s is the soil effective thermal conductivity and $\rho_s c_s$ is given in Eq. 6. If we assume that λ_s and $\rho_s c_s$ are both homogeneous in the vertical direction, then Eq. 16 can be rewritten as

$$\frac{\partial T}{\partial t} = k\frac{\partial^2 T}{\partial z^2}, \quad (18)$$

$$k = \frac{\lambda_s}{C_s \rho_s}. \quad (19)$$

Here, k is known as the soil thermal diffusivity.

The numerical formation of the TDE is described in Yang and Wang (2008). The observed soil temperatures at the land surface (z=0) and at a depth of 0.40 m are set as the boundary conditions. The number of layers in the model is 80; the depths of the upper layers are smaller than the lower layers. The component of dry soil is assumed to be uniform above 0.40 m. λ_s is given by the following:

$$\lambda_s = (1\text{-}\theta_{sat})\lambda_{dry} + \theta\lambda_w + (\theta_{sat} - \theta)\lambda_a, \quad (20)$$

where λ_w and λ_a are the thermal conductivity of liquid water and air in the soil, set to be 0.60 (unit: W m^{-1} K^{-1}) and 0.023, respectively. λ_{dry} is not the pure thermal conductivity of dry soil but represents part of the heat transfer by liquid and vapor water as well. With this consideration, an optimal λ_s can be determined though comparing the bias from different simulated cases with different λ_{dry}.

The simulation deviation at each level is defined as

$$T_{ba}(t,z) = T_{ob}(t,z) - T_c(t,z), \quad (21)$$

where T_{ob} represents the observation and T_c represents the calculated value from the TDE. The root-mean-square deviation is defined as

$$\delta(z) = \frac{\sqrt{\sum_{t=1}^{n_t} T_{ba}(t,z)^2}}{n_t - 1}, \quad (22)$$

where n_t represents the number of observation samples. Considering the observation level (Table 1), the simulation is compared with observations at depths of 0.05, 0.10, and 0.20 m.

The δ at three levels for different λ_{dry} values is given in Table 2. The δ at a depth of 0.05 m is smallest when λ_{dry}=1.0, but is much greater at other depths. The sum of δ at the three

Table 2 Root-mean-square deviation of soil temperature (δ, units: 10^{-3} K) from the TDE in the cases with different thermal conductivities of dry soil (λ_{dry}, units: W m^{-1} K^{-1})

	0.8	1.0	1.2	…	2.2	2.4	2.6	…	3.5	3.7	3.9
Z=0.05	6.98	**6.94**	6.97	…	7.75	7.99	8.24	…	9.46	9.74	10.0
Z=0.10	1.99	1.82	1.66	…	1.07	**1.04**	1.05	…	1.50	1.66	1.82
Z=0.20	0.99	0.93	0.87	…	0.59	0.53	0.48	…	0.32	**0.31**	0.33

The minimum in each row is in bold

levels is smallest when λ_{dry}=1.2. Fig. 6 shows the daily averaged diurnal variation of T_{ba} at a depth of 0.05 m in three cases. Between 0800 and 1700, the T_{ba} in all three cases is positive, meaning that the simulated soil temperature is lower than observed. However, during other periods, the situation is opposite. The phase of T_{ba} in different simulations is similar, indicating that the cause may be the same.

To discuss the cause of T_{ba}, the temperature control equation for the real soil can be written as

$$\frac{\partial \rho_s c_s T_{ob}}{\partial t} = \frac{\partial}{\partial z}\left(\lambda_s \frac{\partial T_{ob}}{\partial z}\right) + Q. \tag{23}$$

Here, Q is the heating/cooling process that was not considered well in the TDE. After replacing T with T_c in Eq. 16, we subtract Eq. 16 from Eq. 23 to arrive at

$$\frac{\partial \rho_s c_s T_{ba}}{\partial t} = \frac{\partial}{\partial z}\left(\lambda_s \frac{\partial T_{ba}}{\partial z}\right) + Q. \tag{24}$$

The first term on the right-hand side of Eq. 24 cannot be precisely calculated because the T_{ba} at depths of 0.05, 0.10, and 0.20 m only can be given. For a qualitative analysis, we ignore this term to obtain

$$\frac{\partial T_{ba}}{\partial t} \approx \frac{Q}{\rho_s c_s}. \tag{25}$$

Equation 25 indicates that Q should be identical to the variability of T_{ba}. Thus, from Fig. 6, when T_{ba} increases from 0800 to 1000, Q should be positive and corresponding to a heating process, while after 1000, a cooling process.

5.2 Simplification of internal evaporation and condensation

Basing on the surface energy analysis in the previous section, internal evaporation and condensation can be presented as a soil moisture change rate (θ_t) (Eq. 14). With this consideration, the control equation for the soil temperature in the presence of internal evaporation and/or condensation can be simply given as

$$\frac{\partial \rho_s c_s T}{\partial t} = \frac{\partial}{\partial z}\left(\lambda_s \frac{\partial T}{\partial z}\right) + l\rho_w \theta_t p'. \tag{26}$$

Here, p' is introduced to represent the proportion of evaporation- and/or condensation-induced soil moisture change. From Eq. 14, p' should be proportional to the reciprocal of p. Compared with Eq. 25, the following should hold:

$$T_{ba} \approx C\theta + \text{constant}, \tag{27a}$$

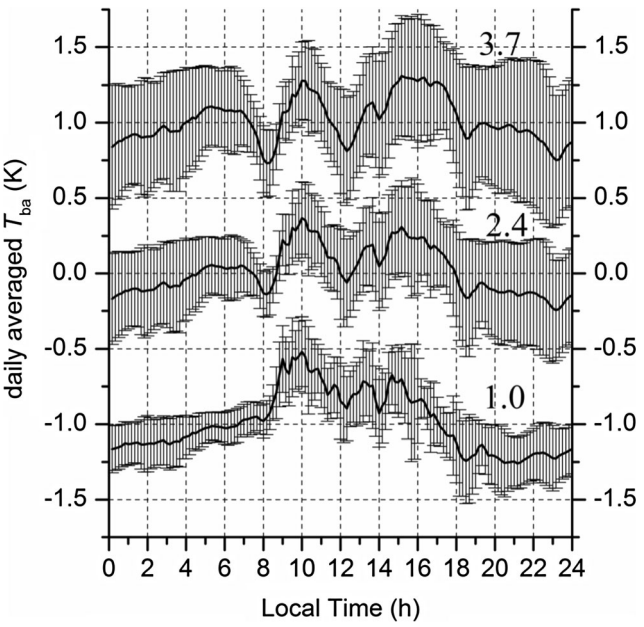

Fig. 6 The 11-day averaged diurnal variation of simulation deviation (T_{ba}) at a depth of 0.05 m from simulation cases with λ_{dry} being equal to 1.0, 2.4, and 3.7 (see Eq. 20). The results for λ_{dry} equal to 1.0 and 3.7 have had −1 and 1 added to them, respectively

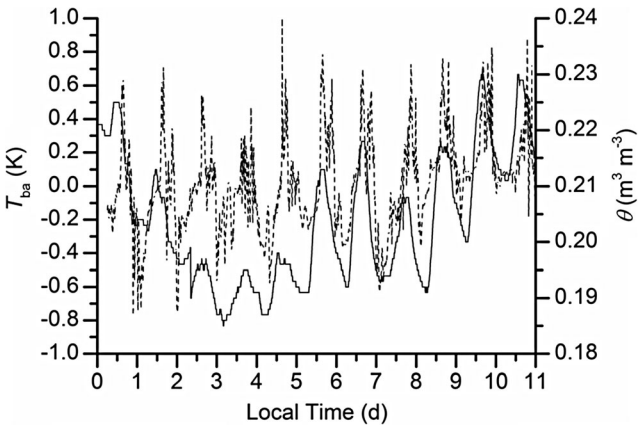

Fig. 7 Daily variation of observed soil moisture (θ, *solid line*) and T_{ba} (*dashed line*) with λ_{dry}=1.0 at a depth of 0.05 m from June 27 to July 7, 2005

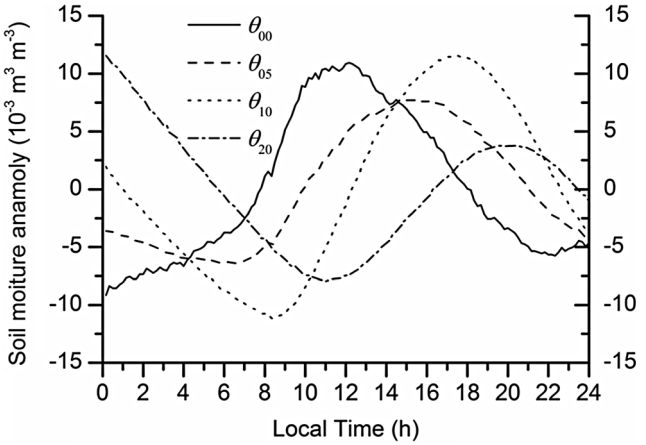

Fig. 8 Daily averaged diurnal variation of soil moisture at depths of 0.0 m (θ_{00}), 0.05 m (θ_{05}), 0.10 m (θ_{10}), and 0.20 m (θ_{20}). θ_{00} is linearly extrapolated from θ_{05} and θ_{00}. The mean values at the four levels, which are 0.10, 0.20, 0.31, and 0.41, respectively, have all been subtracted

$$C = \frac{l\rho_w p'}{\rho_s c_s}. \tag{27b}$$

The daily variation of T_{ba} (λ_{dry}=2.4) and θ at a depth of 0.05 m from June 27 to July 7 are given in Fig. 7, and their mean diurnal variation is given in Fig. 8. Obviously, their identical diurnal variation partly confirms Eq. 27a. The surface soil moisture (θ_{00}) is calculated by linear extrapolation from the observation at the depths of 0.05 and 0.10 m. With increasing depth, the phases of soil moisture are delayed but the amplitudes do not decay. If the intensity of internal evaporation and condensation decays exponentially with depth, then p' can be given as

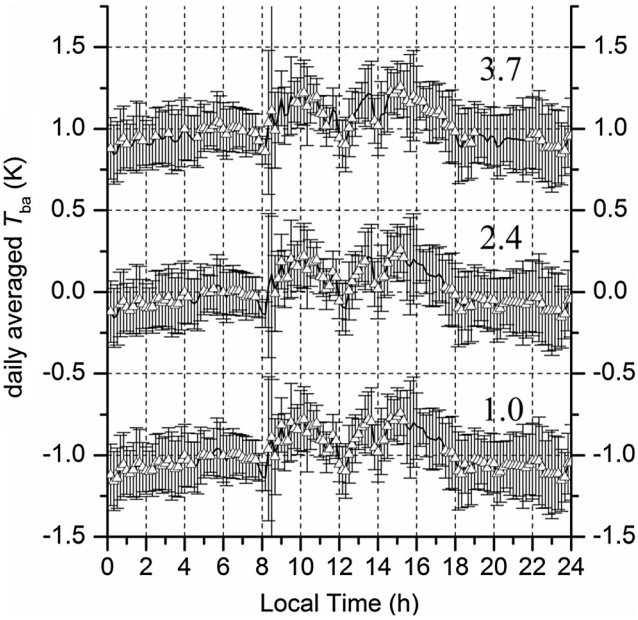

Fig. 9 As in Fig. 6 but for the results of the TDE_EC (D_w=0.03). *Triangles* show where the absolute value of the daily averaged T_{ba} from TDE_EC is smaller than those obtained from the TDE

$$p' = \exp\left(-\frac{z}{D_w}\right). \tag{28}$$

Here, D_w is the *e*-folding depth for internal evaporation and condensation. Equation 28 suggests that both internal condensation and evaporation will concentrate near the surface. Putting Eq. 28 into Eq. 26 and using the same settings and boundary conditions as in the TDE, we can reproduce the soil

Table 3 Root-mean-square deviation (δ, units: 10^{-3} K) at different levels from the TDE_EC in cases with different thermal conductivities (λ_{dry}, units: W m^{-1} K^{-1}) and D_w (see Eq. 27, units: m)

D_w		λ_{dry}=0.3	0.4	0.5	0.6	0.7	0.8	0.9	1.0	1.5	2.0	2.5	3.9
0.01	Z=0.05	5.48	5.42	**5.39**	5.40	5.43	5.48	5.56	5.66	6.35	7.24	8.21	10.8
	Z=0.10	2.70	2.58	2.46	2.35	2.22	2.12	2.00	1.90	1.43	**1.12**	1.12	2.32
	Z=0.20	1.14	1.11	1.08	1.04	0.99	0.97	0.94	0.90	0.74	0.57	0.43	**0.42**
0.02	Z=0.05	5.07	**5.05**	5.06	5.09	5.15	5.23	5.34	5.47	6.27	7.23	8.23	10.9
	Z=0.10	2.66	2.54	2.42	2.30	2.19	2.07	1.96	1.86	1.39	**1.10**	1.16	2.41
	Z=0.20	1.14	1.11	1.08	1.04	1.00	0.97	0.94	0.90	0.74	0.57	0.43	**0.42**
0.03	Z=0.05	**4.75**	4.77	4.82	4.90	5.00	5.12	5.26	5.41	6.32	7.35	8.39	11.09
	Z=0.10	2.53	2.41	2.29	2.18	2.07	1.96	1.85	1.75	1.33	**1.17**	1.33	2.67
	Z=0.20	1.14	1.11	1.07	1.04	0.99	0.96	0.93	0.90	0.73	0.57	0.43	**0.42**
0.04	Z=0.05	**4.77**	4.82	4.90	5.01	5.14	5.28	5.44	5.61	6.57	7.62	8.66	11.35
	Z=0.10	2.41	2.30	2.19	2.09	1.99	1.90	1.81	1.73	1.44	**1.43**	1.70	3.08
	Z=0.20	1.14	1.10	1.07	1.03	1.00	0.96	0.93	0.90	0.73	0.58	0.42	**0.42**
0.05	Z=0.05	**5.01**	5.08	5.19	5.30	5.44	5.60	5.77	5.95	6.92	7.94	8.98	11.61
	Z=0.10	2.40	2.30	2.22	2.14	2.06	2.00	1.93	1.88	**1.75**	1.87	2.19	3.56
	Z=0.20	1.14	1.10	1.07	1.03	1.00	0.97	0.94	0.90	0.74	0.58	0.44	**0.44**

The minimum value in each row is in bold

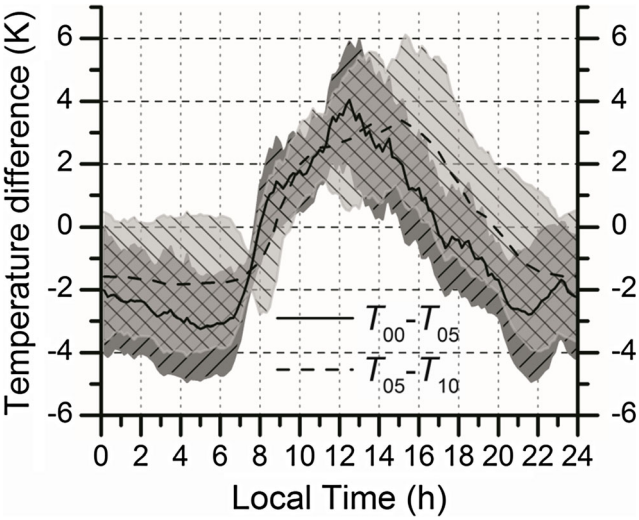

Fig. 10 Daily averaged diurnal variation of soil temperature difference between the surface and a depth of 0.05 m (T_{00}–T_{05}) and between the depths of 0.05 and 0.10 m (T_{05}–T_{10}). The *hatched shading* shows their standard deviations

temperature. The thermal diffusion equations with internal evaporation and condensation are indicated as TDE_EC.

The reproduced soil temperature from TDE_EC is much closer to the observation (Table 3). The most significant improvements take place in the upper layer (0.05 m) where δ has been reduced by 30 %. The δ at 0.10 m becomes worse than in the TDE method, but remains acceptable. The δ at 0.20 m changes little because the water distillation there is weak. It should be noted that the optimized λ_s in TDE_EC tends to be smaller than that in the TDE. This is because the distillation has been separately considered, and thus, λ_s in TDE_EC should be closer to the pure soil conductivity rather than the effective conductivity in the TDE. To demonstrate the improvement of TDE_EC, its daily averaged T_{ba} is given in Fig. 9. For different λ_{dry} quantities, the simulation of TDE_EC is closer to the observations during most periods than that from the TDE. This indicates that the distillation process should be robust in the shallow soil layer during the experiment periods.

Therefore, relying on the selection of a proper effective thermal conductivity is insufficient to successfully represent the heat transfer in soil due to water distillation. Instead, when a part of the soil moisture change is accounted for by internal evaporation and condensation, the numerical reproduction of soil temperature becomes much improved, especially in the shallow soil layer.

6 Discussion

Besides water distillation, the vertical liquid water flux in soil also impacts both the soil temperature and moisture and is thus referred to as soil thermal convection (Gao 2005; Gao et al. 2003). The inclusion of thermal convection in the TDE can be represented by

$$\frac{\partial \rho_s c_s T}{\partial t} = \frac{\partial}{\partial z}\left(\lambda_s \frac{\partial T}{\partial z}\right) - \rho_w c_w w \theta \frac{\partial T}{\partial z}, \tag{29}$$

where w is the vertical speed of the liquid water, positive being upward. If there are no liquid water supplements, such as precipitation and irrigation, w is positive during daytime because the water evaporated at the land surface needs to be balanced. Therefore, the vertical gradient of soil temperature will determine the heating rate of thermal convection.

Figure 10 shows the observed soil temperature difference between the surface and a depth of 0.05 m and between the depths of 0.05 and 0.10 m. The temperature gradient between 0.05 and 0.10 m is negative from 0800 to 0900. Therefore, the thermal convection will indeed heat the soil at a depth of 0.05 m. However, the soil temperature in the upper layer is

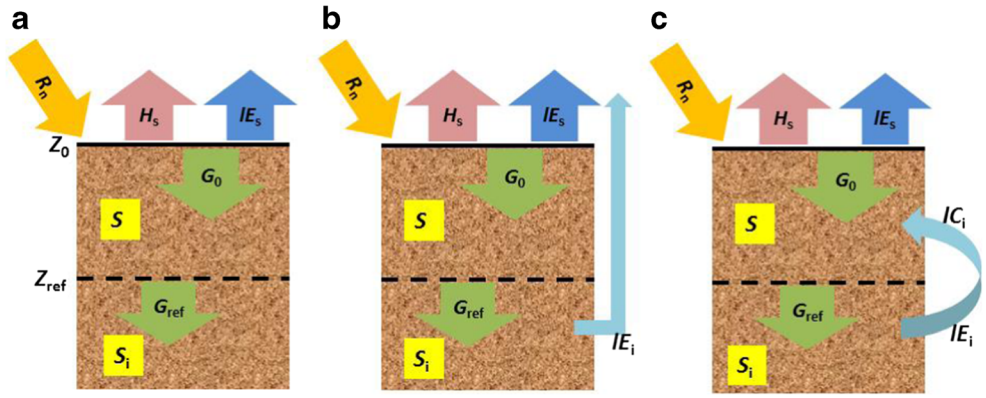

Fig. 11 Diagrams to show the effect of internal evaporation/condensation within soil on the observation of surface energy balance. All *arrows* stand for energy fluxes. The two *yellow boxes* stand for the soil heat storage rate: S for the layer from Z_0 to Z_{ref} and S_i for the layer under Z_{ref}. In **a**, there is no internal evaporation/condensation; Eq. 3 (S=G_0–G_{ref}) is true in this situation. In **b**, there is internal evaporation happening in the soil, which should follow lE_i=G_{ref}–S_i. In **c**, all water vapor flux generated through internal evaporation (lE_i) has been condensed (lC_i) in the layer above Z_{ref}; Eq. 11 is true in this situation

usually higher than that in the lower layer for most of the daytime. This means that thermal convection tends to cool the soil at a depth of 0.05 m, which is not expected from previous analysis. Furthermore, what may be more important is that the second term on the right-hand side of Eq. 29 is too small (~1 W m^{-2} within a depth of 0.4 m) than observed R. Therefore, the liquid water flux may not be the main cause for the bias of soil temperature in the TDE.

Besides hydrothermal processes in soil, the variation of water in plant roots might also affect the soil moisture observed (Cowan 1965; Huck et al. 1970; Laio et al. 2001; Priesack et al. 2012). Thus, it may partly contribute to the observed diurnal variation of soil moisture, but it cannot cause such a significant R. Therefore, compared with previous studies on water distillation in soil (Bittelli et al. 2008; Bouddour et al. 1998), this study is based more on field observations.

The most intense condensation in shallow soil is suggested to occur in the early morning (from 0800 to 1000 LST) in the Jinta oasis. This seems to be different from previous reports based on lysimeter observations (Jacobs et al. 1999, 2006, 2008). In these studies, the internal condensation mainly occurred at nighttime, and the soil was losing water during the daytime. However, it should be noted that only the distillation in the shallow soil layer (above the heat flux plate) can be reflected in surface energy balance analysis. In fact, even when the internal condensation is strong in shallow soil, the whole soil column is still losing water through evaporation (Fig. 2).

7 Conclusion

This study found that, in the Jinta oasis experiment, the observed soil heat storage above 0.05 m between 0800 and 1000, as well as the significant negative imbalanced energy flux during daytime, can be explained by the impact of internal condensation and evaporation, respectively.

To further clarify the main mechanism of internal evaporation and condensation involved, we provide simple diagrams in Fig. 11. The general situation for the surface energy flux balance is presented in Fig. 11a, within which the water distillation can be neglected. When there is significant internal evaporation but no condensation (Fig. 11b), the eddy covariance system will erroneously count the internal evaporation, which is generated in the soil layer under Z_{ref}, as the total surface evaporation, causing a negative imbalanced energy flux. If all water vapor flux generated by internal evaporation has been condensed in the soil layer above Z_{ref} (Fig. 11c), then the soil heat storage in the layer above Z_{ref} cannot be used to derive the soil heat flux at the surface (G_0), as suggested by previous studies (Culf et al. 2004; Foken et al. 2006; Garratt 1994). We suggest that about 70 % of the soil moisture variability above a depth of 0.05 m can be attributed to water distillation in the Jinta oasis.

In order to show the importance of water distillation within soil, the soil temperature was reproduced using a one-dimensional thermal diffusion equation. Even after the thermal effective conductivity was optimized, the bias of simulated shallow soil temperature could be reduced by about 30 % after the water distillation was considered to be proportional to the soil moisture variability in the shallow soil layer.

Acknowledgments We appreciate the faculty of the Jinta experiment for their hard work to collect and quantify all observation data. We also feel grateful for the two anonymous reviewers and editor; their criticism and comments have greatly helped us to improve this paper. This research was funded by the National Natural Science Foundation of China (Grant No. 41205005, 41130961) and the West Light Foundation of the Chinese Academy of Sciences (for Han Bo).

References

Agam N, Berliner PR (2006) Dew formation and water vapour adsorption in semi-arid environments—a review. J Arid Environ 65(4):572–590

Andrade JL (2003) Dew deposition on epiphytic bromeliad leaves: an important event in a Mexican tropical dry deciduous forest. J Trop Ecol 19:479–488

Ao Y, Lu S, Han B, Li Z (2014) Comparative analysis of the soil thermal regimes of typical underlying surfaces of oasis systems in an arid region. Environ Earth Sci. doi:10.1007/s12665-014-3937-7

Bastiaanssen WGM, Pelgrum H, Wang J, Ma Y, Moreno JF, Roerink GJ, van der Wal T (1998) A remote sensing surface energy balance algorithm for land (SEBAL)—2. Validation J Hydrol 212(1–4): 213–229

Beltrán Przekurat A, Pielke RA Sr, Eastman JL, Coughenour MB (2012) Modelling the effects of land-use/land-cover changes on the near-surface atmosphere in southern South America. Int J Climatol 32(8): 1206–1225

Bittelli M, Ventura F, Campbell GS, Snyder RL, Gallegati F, Pisa PR (2008) Coupling of heat, water vapor, and liquid water fluxes to compute evaporation in bare soils. J Hydrol 362(3–4):191–205

Bouddour A, Auriault J-L, Mhamdi-Alaoui M, Bloch J-F (1998) Heat and mass transfer in wet porous media in presence of evaporation–condensation. Int J Heat Mass Transf 41(15):2263–2277

Chu PC, Lu SH, Chen YC (2005) A numerical modeling study on desert oasis self-supporting mechanisms. J Hydrol 312(1–4):256–276

Cowan I (1965) Transport of water in the soil-plant-atmosphere system. J Appl Ecol :221–239

Culf AD, Foken T, Gash GH et al (2004) The energy balance closure problem. In: Kabat P (ed) Vegetation, water, humans and the climate. A new perspective on an interactive system, Global Change—The IGBP Series. Springer, Berlin, pp 159–166

De Vries D (1958) Simultaneous transfer of heat and moisture in porous media. Trans AGU 39:909–916

De Vries D, Philip J (1986) Soil heat flux, thermal conductivity, and the null-alignment method. Soil Sci Soc Am J 50(1):12–18

Deru MP, Kirkpatrick AT (2002) Ground-coupled heat and moisture transfer from buildings. Part 1—analysis and modeling. J Sol Energ-T Asme 124(1):10–16

Devries DA (1987) The theory of heat and moisture transfer in porous-media revisited. Int J Heat Mass Transf 30(7):1343–1350

Foken T (2008) The energy balance closure problem: an overview. Ecol Appl 18(6):1351–1367
Foken T, Wimmer F, Mauder M, Thomas C, Liebethal C (2006) Some aspects of the energy balance closure problem. Atmos Chem Phys 6: 4395–4402
Foken T et al (2010) Energy balance closure for the LITFASS-2003 experiment. Theor Appl Climatol 101(1–2):149–160
Fritschen L, Doraiswamy P (1973) Dew: an addition to the hydrologic balance of Douglas fir. Water Resour Res 9(4):891–894
Gao ZQ (2005) Determination of soil heat flux in a Tibetan short-grass prairie. Bound-Layer Meteorol 114(1):165–178
Gao ZQ, Fan XG, Bian LG (2003) An analytical solution to one-dimensional thermal conduction-convection in soil. Soil Sci 168(2):99–107
Garratt JR (1994) The atmospheric boundary layer. Cambridge university press
Garratt JR, Segal M (1988) On the contribution of atmospheric moisture to dew formation. Bound-Layer Meteorol 45(3):209–236
Grifoll J, Gasto JM, Cohen Y (2005) Non-isothermal soil water transport and evaporation. Adv Water Resour 28(11):1254–1266
Han B, Lu SH, Ao YH (2010) Analysis on the interaction between turbulence and secondary circulation of the surface layer at Jinta oasis in summer. Adv Atmos Sci 27(3):605–620
Heitman JL, Horton R (2011) Coupled heat and water transfer in soil. In: Encyclopedia of Agrophysics. Springer, pp 155–162
Henry HAL (2007) Soil freeze-thaw cycle experiments: trends, methodological weaknesses and suggested improvements. Soil Biol Biochem 39(5):977–986
Henry HAL (2008) Climate change and soil freezing dynamics: historical trends and projected changes. Clim Chang 87(3–4):421–434
Heusinkveld BG, Jacobs AFG, Holtslag AAM, Berkowicz SM (2004) Surface energy balance closure in an arid region: role of soil heat flux. Agric For Meteorol 122(1–2):21–37
Huck MG, Klepper B, Taylor HM (1970) Diurnal variations in root diameter. Plant Physiol 45(4):529–530
Hunt AG, Ewing RP, Horton R (2013) What's wrong with soil physics? Soil Sci Soc Am J 77(6):1877–1887
Jacobs AFG, Pul WV, Dijken AV (1990) Similarity of moisture dew profiles within a corn canopy. J Appl Meteorol 29(12):1300–1306
Jacobs AFG, Heusinkveld BG, Berkowicz SM (1999) Dew deposition and drying in a desert system: a simple simulation model. J Arid Environ 42(3):211–222
Jacobs AFG, Heusinkveld BG, Kruit RJW, Berkowicz SM (2006) Contribution of dew to the water budget of a grassland area in the Netherlands. Water Resour Res 42(3), W03415
Jacobs AFG, Heusinkveld BG, Holtslag AAM (2008) Towards closing the surface energy budget of a mid-latitude grassland. Bound-Layer Meteorol 126(1):125–136
Johansen O (1977) Thermal conductivity of soils. DTIC Document
Johnson A, Roy IM, Matthews GP, Patel D (2003) An improved simulation of void structure, water retention and hydraulic conductivity in soil with the Pore-Cor three-dimensional network. Eur J Soil Sci 54(3):477–489
Kondo J, Saigusa N, Sato T (1990) A parameterization of evaporation from bare soil surfaces. J Appl Meteorol 29(5):385–389
Laio F, Porporato A, Ridolfi L, Rodriguez-Iturbe I (2001) Plants in water-controlled ecosystems: active role in hydrologic processes and response to water stress—II. Probabilistic soil moisture dynamics. Adv Water Resour 24(7):707–723
Li Q, Sun SF (2008) Development of the universal and simplified soil model coupling heat and water transport. Sci China Ser D 51(1):88–102
Massmann J, Farrier DF (1992) Effects of atmospheric pressures on gas-transport in the vadose zone. Water Resour Res 28(3):777–791
Milly PCD (1984) A simulation analysis of thermal effects on evaporation from soil. Water Resour Res 20(8):1087–1098
Moeng CH, Sullivan PP (1994) A comparison of shear-driven and buoyancy-driven planetary boundary-layer flows. J Atmos Sci 51(7):999–1022
Monteith J (1965) Evaporation and environment. Symp Soc Exp Biol 19: 205–234
Nassar I, Globus A, Horton R (1992) Simultaneous soil heat and water transfer. Soil Sci 154(6):465–472
Ninari N, Berliner PR (2002) The role of dew in the water and heat balance of bare loess soil in the Negev Desert: quantifying the actual dew deposition on the soil surface. Atmos Res 64(1–4):323–334
Oke TR, Spronken-Smith RA, Jauregui E, Grimmond CSB (1999) The energy balance of central Mexico City during the dry season. Atmos Environ 33(24–25):3919–3930
Olivella S, Gens A, Carrera J (2000) Water phase change and vapour transport in low permeability unsaturated soils with capillary effects. In: JM C (ed) Computational methods for flow and transport in porous media. Theory and Applications of Transport in Porous Media. Springer, Netherlands, pp 245–272
Oncley SP et al (2007) The energy balance experiment EBEX-2000. Part I: overview and energy balance. Bound-Layer Meteorol 123(1):1–28
Ong SK, Culver TB, Lion LW, Shoemaker CA (1992) Effects of soil-moisture and physical-chemical properties of organic pollutants on vapor-phase transport in the vadose zone. J Contam Hydrol 11(3–4): 273–290
Penman HL (1948) Natural evaporation from open water, bare soil and grass. Proc R Soc Lond A 193(1032):120–145
Philip JR (1957) Evaporation, and moisture and heat fields in the soil. J Meteorol 14(4):354–366
Philip JR, De Vries DA (1957) Moisture movement in porous materials under temperature gradients. Trans Am Geophys Union 38:222–232
Poutou E, Krinner G, Genthon C, de Noblet-Ducoudre N (2004) Role of soil freezing in future boreal climate change. Clim Dyn 23(6):621–639
Priesack E, Gayler S, Rötzer T, Seifert T, Pretzsch H (2012) Mechanistic modelling of soil–plant–atmosphere systems. In: Matyssek R, Schnyder H, Oßwald W, Ernst D, Munch J, Pretzsch H (eds) Growth and defence in plants. Resource allocation at multiple scales. Ecological studies. Springer, Berlin, pp 335–353
Qi SZ, Li XY, Duan HP (2007) Oasis land-use change and its environmental impact in Jinta Oasis, arid northwestern China. Environ Monit Assess 134(1–3):313–320
Ren D, Leslie LM, Karoly DJ (2008) Sensitivity of an ecological model to soil moisture simulations from two different hydrological models. Meteorog Atmos Phys 100(1–4):87–99
Richards K (2004) Observation and simulation of dew in rural and urban environments. Prog Phys Geogr 28(1):76–94
Saito H, Simunek J, Mohanty BP (2006) Numerical analysis of coupled water, vapor, and heat transport in the vadose zone. Vadose Zone J 5(2):784–800
Sakai RK, Fitzjarrald DR, Moore KE (2001) Importance of low-frequency contributions to eddy fluxes observed over rough surfaces. J Appl Meteorol 40(12):2178–2192
Sakai M, Toride N, Simunek J (2009) Water and vapor movement with condensation and evaporation in a sandy column. Soil Sci Soc Am J 73(3):707–717
Scanlon BR (1992) Evaluation of liquid and vapor water flow in desert soils based on chlorine 36 and tritium tracers and nonisothermal flow simulations. Water Resour Res 28(1):285–297
Scanlon BR (1994) Water and heat fluxes in desert soils.1. Field studies. Water Resour Res 30(3):709–719
Scanlon BR, Milly PCD (1994) Water and heat fluxes in desert soils.2. Numerical simulations. Water Resour Res 30(3):721–733
Shao YP, Irannejad P (1999) On the choice of soil hydraulic models in land-surface schemes. Bound-Layer Meteorol 90(1):83–115

Sharma ML (1976) Contribution of dew in the hydrologic balance of a semi-arid grassland. Agric Meteorol 17(5):321–331

Simunek J, van Genuchten MT, Sejna M (2008) Development and applications of the HYDRUS and STANMOD software packages and related codes. Vadose Zone J 7(2):587–600

Sundberg J (1988) Thermal properties of soils and rocks

Tarnawski VR, Gori F, Wagner B, Buchan GD (2000) Modelling approaches to predicting thermal conductivity of soils at high temperatures. Int J Energy Res 24(5):403–423

Tsukamoto O, Sahashi K, Wang J (1995) Heat budget and evapotranspiration at an oasis surface surrounded by desert: special edition on HEIFE. I. J Meteorol Soc Jpn 73(5):925–935

Tuller M, Or D, Dudley LM (1999) Adsorption and capillary condensation in porous media: liquid retention and interfacial configurations in angular pores. Water Resour Res 35(7):1949–1964

Waggoner PE, Begg JE, Turner NC (1969) Evaporation of dew. Agric Meteorol 6(3):227–230

Wang JM, Mitsuta Y (1992) Evaporation from the desert: some preliminary results of HEIFE. Bound-Layer Meteorol 59(4):413–418

Wang M, Wang J, Pan N, Chen S, He J (2007) Three-dimensional effect on the effective thermal conductivity of porous media. J Phys D Appl Phys 40(1):260

Wilson K et al (2002) Energy balance closure at FLUXNET sites. Agric For Meteorol 113(1–4):223–243

Wu W, Dickinson RE, Wang H, Liu Y, Shaikh M (2007) Covariabilities of spring soil moisture and summertime United States precipitation in a climate simulation. Int J Climatol 27(4):429–438

Xiao H, Meissner R, Seeger J, Rupp H, Borg H (2009) Effect of vegetation type and growth stage on dewfall, determined with high precision weighing lysimeters at a site in northern Germany. J Hydrol 377(1–2):43–49

Yang K, Wang J (2008) A temperature prediction-correction method for estimating surface soil heat flux from soil temperature and moisture data. Sci China Ser D 51(5):721–729

Yang K, Koike T, Ye B, Bastidas L (2005) Inverse analysis of the role of soil vertical heterogeneity in controlling surface soil state and energy partition. J Geophys Res-Atmos 110(D8), D08101

Zeng YJ, Wan L, Su ZB, Saito H, Huang KL, Wang XS (2009) Diurnal soil water dynamics in the shallow vadose zone (field site of China University of Geosciences, China). Environ Geol 58(1):11–23